Fast radiative cooling of anthracene: Dependence on internal energy

S. Martin,[1] M. Ji,[1] J. Bernard,[1] R. Brédy,[1] B. Concina,[1] A. R. Allouche,[1] C. Joblin,[2,3] C. Ortega,[1] G. Montagne,[1] A. Cassimi,[4] Y. Ngono-Ravache,[4] and L. Chen[1,*]

[1]*Institut Lumière Matière, UMR5306, Université Lyon 1-CNRS, Université de Lyon, 69622 Villeurbanne Cedex, France*

[2]*Université de Toulouse, UPS-OMP, IRAP, Toulouse, France*

[3]*CNRS, IRAP, 9 Avenue Colonel Roche, BP 44346, F-31028 Toulouse Cedex 4, France*

[4]*CIMAP, CEA/CNRS/ENSICAEN/Université Caen Normandie, Boulevard H. Becquerel, BP 5133, F-14070 Caen cedex 5, France*

(Received 17 July 2015; published 25 November 2015)

Fast radiative cooling of anthracene cations $(C_{14}H_{10})^+$ is studied with a compact electrostatic storage device, the Mini-Ring. The time evolution of the internal energy distribution of the stored ions is probed in a time range from 3 to 7 ms using laser-induced dissociation with 3.49-eV photons. The population decay rate due to radiative emission is measured to vary from 25 to 450 s^{-1} as a function of the excitation energy in the range from 6 to 7.4 eV. After corrections of the infrared emission effect via vibrational transitions, the fluorescence emission rate due to electronic transitions from thermally excited electronic states is estimated and compared with a statistical molecular approach. In the considered internal energy range, the radiative cooling process is found to be dominated by the electronic transition, in good agreement with our previous work [S. Martin *et al.*, Phys. Rev. Lett. **110**, 063003 (2013)] focused on a narrower energy range.

DOI: 10.1103/PhysRevA.92.053425 PACS number(s): 37.10.Mn, 33.80.−b, 37.10.Pq, 95.30.Ft

I. INTRODUCTION

Polycyclic aromatic hydrocarbon (PAH) molecules are key chemical species in astrophysics, combustion, and environmental studies. The ubiquitous presence of PAH molecules in the interstellar medium (ISM) was proposed 30 years ago [1,2] and has motivated a considerable effort in the laboratory to study the physical and chemical properties of these species (see [3] for a compilation of studies). Polycyclic aromatic hydrocarbon molecules in the ISM are revealed by emission in specific IR bands following the absorption of UV photons. Their survival depends then on the competition between the two main energy decay routes: the unimolecular dissociation and radiative cooling. It is generally admitted that after absorption of a UV photon, internal conversion from the electronic excited state followed by intermolecular vibrational distribution in the ground electronic state leads to hot molecules. The IR cooling rate has been calculated to be in the range from ∼1 to ∼10 s^{-1} without a strong dependence on size. With such a slow radiative decay mechanism, PAH molecules are expected to experience severe photodissociation unless they are large enough (more than 50 carbon atoms according to [4]). Léger *et al.* considered an additional radiative decay mechanism that would lead to faster radiative cooling especially at high energies [5,6]. This mechanism is based upon the fact that excited electronic states may be populated by interaction with the electronic ground state at high enough internal energy due to inverse internal conversion. Even though the population probability is very low, the Einstein coefficient for spontaneous electronic transition of such excited states could be several orders of magnitude larger than the IR vibrational emission rate leading to faster cooling via visible fluorescence emission. The latter is called Poincaré fluorescence in [5] and its first indirect evidence was reported for the PAH cation anthracene $C_{14}H_{10}^+$ [7]. In more recent works on this small PAH molecule, the fast radiative decay rate of the anthracene cation was measured [8] and calculations of its structure and spectral properties were performed [9]. A similar radiative decay process has been referred to as fluorescence from thermally excited electronic states in studies on large molecules such as fullerenes [10–12] and on small cluster anions Al_n^- ($n = 4$–5) [13,14]. Studies on small carbonaceous anions, namely, C_5^-, C_6^-, C_6H^-, and C_7^-, have demonstrated the dramatic effect of the electronic structure on radiative cooling, which was found to be limited to IR emission in the case of C_5^- and C_6H^- and much faster for the other species due to the fluorescence from electronic states [15–17]. For fullerene and metal clusters, radiative cooling rates from electronic states were calculated using a dielectric model based on a plasmon description [18]. For anthracene, Boissel *et al.* [7] used a statistical molecular approach to estimate the population probability of the excited states and their emission rates. They showed that the calculated cooling rate allowed them to account for the evolution of the fragmentation efficiency with the period of modulation of the UV light.

A direct way to obtain the electronic fluorescence rate would involve the detection of the emitted (visible or near-IR) photons. However, despite it being a fast cooling process compared to IR emission, this fluorescence is actually slow with a typical lifetime larger than 1 ms. Ion storage techniques are needed to study decay processes on such a time scale. Linear or bend electrostatic ion-beam storage traps (EIBT) or rings [19–28] have been developed to study the dynamics of delayed photofragmentation, electron photodetachment, and photoionization processes for time scales between microseconds and a few tens of milliseconds. With these devices, it becomes possible to get insight into cooling rates by monitoring neutral dissociation products and following the evolution of the internal energy distribution (IED) of the stored molecular ensemble. We constructed a small electrostatic storage ring (ESR) [27], called Mini-Ring, which combined the advantages of the large ESRs and the small EIBTs. Similarly to larger ESR experiments, the stored ions can be excited

*chen@univ-lyon1.fr

along one of the straight sections (of 9.2 cm long) by a laser beam. Neutral fragments resulting from dissociation processes occurring at the opposite straight section can be detected as a function of time. Due to the compactness of this device and the short ion revolution period (a few microseconds), we are able to measure the laser-induced dissociation in a typical time range from the very first microsecond to about 1ms after laser excitation. Compared with larger rings with a much longer revolution period, the Mini-Ring is very sensitive to the high-energy part of the IED of the stored molecular ion ensemble.

In this paper we focus on the radiative cooling of anthracene cations and its dependence on internal excitation energy. Anthracene cations were stored in the Mini-Ring for such a long time that the dissociation was a negligible process in the experimental time range. The further evolution of the IED of the stored ions was probed by the absorption of a single 3.49-eV photon at different storage times followed by delayed fragmentation. The evolution of the high-energy edge of the IED versus the storage time was analyzed to determine the radiative-emission-induced population decay rate as a function of the energy. The electronic fluorescence rates were derived from the measured population decay rates by correcting the minor contributions of IR emissions. The estimated energy-dependent electronic fluorescence rates were fitted with theoretical values calculated using the Poincaré fluorescence model with a modified spontaneous emission rate.

II. EXPERIMENTAL PROCEDURE

The experimental setup including details about the Mini-Ring has been described in previous papers [27,8]; we give here only a description of the latest updates. The schematic view of the Mini-Ring is shown in Fig. 1. Compared to its earlier design in [27], the setup has been modified in order to improve the experimental conditions. Among the recent developments, we emphasize here the following points.

(i) The kinetic energy of the ion beam has been increased from 2 to 12 keV in order to obtain a better beam shape, higher beam intensity, higher neutral detection efficiency, and weaker betatron oscillation effect.

(ii) Tilted deflection plates ($D_1 - D_4$) (by an angle of 7°) have been installed in order to reduce the noise on the neutral detector and to improve the storage conditions with ion trajectories that remain far enough from the electrode edges.

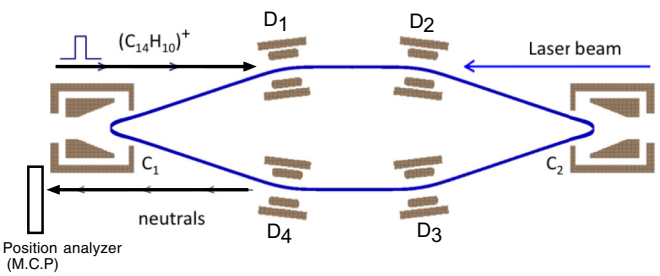

FIG. 1. (Color online) Schematic view of the Mini-Ring composed of two off-axis electrostatic reflectors (C_1 and C_2) and four deflection plates ($D_1 - D_4$). The stored ion trajectory was simulated with the SIMION software.

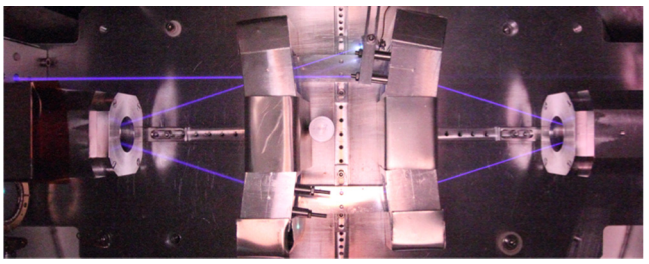

FIG. 2. (Color online) Picture of the Mini-Ring and the trajectory of the Ar^+ ion beam stored for a single turn in the chamber filled with nitrogen gas of pressure about 10^{-4} mbar.

(iii) For neutral detection, the small channeltron electron multiplier has been replaced by a position-sensitive detector (PSD) (Quantar Technology Inc., Santa Cruz CA) composed of two multichannel plates (MCPs) and a resistive anode. This PSD provides a larger collection solid angle and allows for a three-dimensional imaging detection (x, y, t).

(iv) The fragment detection times were recorded using a Lecroy 4208 multihit time-to-digital converter with the resolution of 1 ns and a full time range up to 16 ms. An analog-to-digital converter (AD811 ORTEC) was used to record the X and Y positions of the neutral impact on the PSD. A fast list mode processor Hytec LP1342 was employed to record all events for each storage cycle.

Figure 2 shows a picture of the Mini-Ring in the vacuum chamber. The visible beam trace was obtained using an intense Ar^+ argon ion beam (2 μA) of 12 keV stored for a single revolution in the chamber, which was filled with nitrogen gas at a pressure of about 10^{-4} mbar. The blue light was due to the fluorescence from the N_2 target gas that was excited by collisions with Ar^+ ions along the storage trajectory. A Canon camera (EOS 5D Mark II) equipped with a zoom lens (Ultrasonic 16–35 mm 1:2.8 II USM) was used to take the picture with an exposure time of 10 s. This direct view of the ion trace was helpful for a fine-tuning of the storage conditions. It allowed for *in situ* monitoring of the beam location as a function of the voltages applied to the electrodes in order to drive the ion beam to the optimum trajectory.

A continuous $C_{14}H_{10}^+$ anthracene ion beam of kinetic energy $E_{k0} = 12$ keV with a broad IED was extracted from an electron cyclotron resonance (ECR) NANOGAN ion source. The high-frequency supply of the ECR ion source was operated at very low power (0.2 W) to optimize the intensity of the intact, singly charged $C_{14}H_{10}^+$ ion beam. The beam was mass selected with a 90° magnetic sector and driven into the Mini-Ring chamber with a typical continuous beam intensity of about 1 μA measured on a Faraday cup after one revolution cycle in the ring.

The experiments described in the following were performed using a pulsed beam mode. Beam pulses of short duration, typically 1 μs, were generated every 10 ms by chopping the continuous beam with a parallel plate deflector mounted downstream the mass selection magnet. The flying time of the ions from the ECR source to the Mini-Ring chamber was estimated to be 29 μs. The ion bunches entered then into the ring via the first straight section through D_1 and D_2 and were stored with a revolution period measured to be 6.49 μs.

The evolution of a stored ion bunch was monitored during a storage cycle (10 ms) by recording the time and position at which neutrals exiting the ring through D_4 were impacting the PSD. The electronic pulse applied to the chopper provided the time reference of the subsequent dissociation events for each storage cycle. At the end of each cycle, the remaining ions were ejected from the ring before the entrance of the next bunch. The duration of a storage cycle was chosen much shorter than the storage lifetime limitation due to collisions with the residual gas. The pressure inside the vacuum chamber was maintained under 2×10^{-9} mbar, which ensured a storage lifetime up to 300 ms. This storage lifetime limitation has been found to be relatively independent of the nature of the stored ions. Very similar values have been measured for both atomic ions Ar^+ and molecular PAH ions, namely, singly charged anthracene, naphthalene, and pyrene. Therefore, during a storage cycle, the ion losses resulting from collisions with the residual gas could be considered as a small correction in the analysis.

The Mini-Ring was optimized to store ions within a narrow kinetic energy acceptance window, $\Delta E_k = \pm 40$ eV around $E_{k0} = 12$ keV. By the loss of a small neutral fragment of mass ΔM from the parent molecule of mass M, the kinetic energy of the residual daughter charged fragment is reduced by a quantity $(\Delta M/M)E_{k0}$. In the case where this quantity is smaller than 40 eV, the daughter ion will still be stored in the ring along with the parent ions; otherwise it will be rapidly ejected from the ring. Therefore, the intrinsic kinetic energy acceptance window results in a fragment mass acceptance window $M \pm (\Delta M)_{\max}$, with $(\Delta M)_{\max} = M(|\Delta E_k|/E_{k0}) = M(40/12\,000) = M/300$. The ratio $(\Delta M)_{\max}/M$ is defined as the mass resolution of the ring and is equal to 1/300 in the present experiment. Daughter ions of mass smaller than $M - (\Delta M)_{\max}$ cannot be stored in the ring. It is well known that the anthracene cation ($M = 178$ amu) dissociates mainly via the loss of a neutral H or C_2H_2 [7,29–31] with comparable branching ratios in the range of the internal energy of this work. So, for dissociation events occurring during the storage time, the mass resolution of the ring is sufficient to ensure the ejection of the heavy daughter $(C_{14}H_9)^+$ or $(C_{12}H_8)^+$ fragments from the ring within one additional revolution period.

The detection efficiency of a neutral fragment (mass ΔM) by the PSD depends sensitively on its kinetic energy $(\Delta M/M)E_{k0}$. It was estimated to be about 40% for $C_2H_2(\Delta M = 26)$ with a kinetic energy of 1.753 keV [32] and much smaller for $H(\Delta M = 1)$ estimated to less than 5% due to its much smaller kinetic energy, 70 eV [33]. Moreover, the trajectory of H fragments is expected to be much more sensitive to the kinetic energy release (KER) of the dissociation. The KER for the emission of H was measured to be 0.35 eV for pyrene [34,35] and we have found a comparable value for anthracene. As a consequence, the KER induced significant deviations of the trajectories of the H fragments such that the spot size was larger than the PSD, leading to poor collection efficiency. Due to the reduced detection and collection efficiencies for H fragments, impacts recorded with the PSD were mainly attributed to C_2H_2 neutrals. In a typical spectrum, we plot the number of neutrals (counts) as a function of the storage time (Fig. 3), accumulated over a large number of storage cycles. Neutral count spectra presented in the following were recorded during a typical experimental time

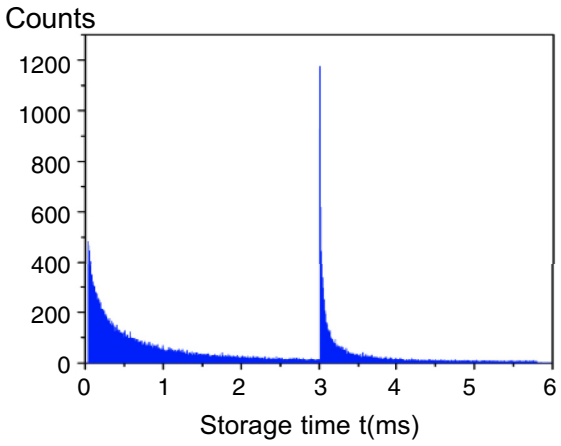

FIG. 3. (Color online) Neutral count spectrum. The number of neutrals as a function of the storage time: $t < 3$ ms, neutral emission due to high-energy population depletion of the broad initial IED from the ECR source; $t > 3$ ms, neutral yield enhancement due to laser excitation at 3 ms.

of one hour corresponding to about 4×10^5 storage cycles. A neutral count rate of 300 counts/s was enough to acquire good statistics. Such a low count rate was maintained to limit the neutral detection number to 3 or 4 per storage cycle so that the probability of having two hits per revolution could be neglected. It also ensured very low ion densities in order to neglect any intrabunch ion-ion scattering effects.

A few milliseconds after the ion injection, at a precise time denoted by t_{laser}, a laser pulse was sent to merge with the ion bunch as the ions passed between deflectors D_1 and D_2. Photon absorption resulted in a sharp and huge enhancement of the neutral count at $t > t_{\text{laser}}$ (Fig. 3). We used nanosecond laser pulses of the third-harmonic Nd:YAG 1-kHz EKSPLA OPO NT242 operated at a 100-Hz repetition rate. The laser beam was unfocused and the size of the spot was estimated to be around 2 mm in diameter along the path between D_1 and D_2. The maximum fluence that we could obtain with this laser at 3.49 eV was about 12 mJ/cm^2 per pulse, however the present spectra were recorded at 2 or 3 mJ/cm^2 per pulse to ensure single-photon-absorption conditions. Adjustments of laser beam paths were realized by translating two plane mirrors mounted on *X*-*Y* microcontrol carriages. In order to optimize both the space and time overlapping between the laser pulse and the ion bunch, neutral counts were recorded as a function of time during the first revolution period after laser excitation with the maximum time resolution (1 ns). The best laser pulse adjustment led to a homogeneous excitation of the ion bunch spreading along the straight line from D_1 to D_2. The signature of such optimized conditions was the recording of a rectangular laser-induced neutral count spectrum (inset in Fig. 4) with a typical width corresponding to the flight time of the ions from D_1 to D_2. The optimized space overlapping conditions were found to be independent of t_{laser} over the total storage time range (<10 ms). This demonstrated that the ion bunch trajectory between D_1 and D_2 was nearly unchanged with the increasing number of revolutions [36] and that the betatron oscillations were considerably reduced compared to the previous measurements [27].

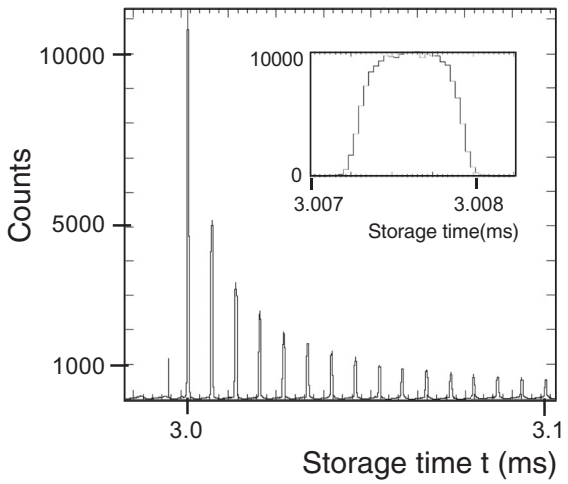

FIG. 4. Neutral count spectrum with one-photon excitation at $t_{laser} = 3$ ms. The inset shows a zoom in of a laser-induced peak showing a rectangular shape and therefore a good overlap between the laser beam and the ion bunch.

III. ANALYSIS OF THE NEUTRAL YIELD DECAY CURVE AT 3 ms

To study the cooling mechanism, one should first prepare anthracene molecular ions to highly excited states. For example, in several previous experiments, thermally evaporated anthracene or other PAH molecules were excited to high energies by UV multiphoton absorption to perform time-resolved photodissociation experiments [37] or by VUV synchrotron radiation absorption to perform threshold photoelectron or imaging photoelectron-photoion coincidence experiments [38,39]. The conditions are very different in our experiment since we started with an ensemble of molecular ions ionized in the plasma of the ECR source with an unknown, probably nonthermalized and broad IED. Molecules with internal energy E may decay via unimolecular dissociation characterized by the dissociation rate $k_{diss}(E)$. Starting from a broad IED at the extraction time ($t = 0$) from the ECR source, the molecules with highest internal energy were dissociated during the first 29 μs along the beam line from the ECR source through the magnet until the Mini-Ring chamber. Although daughter fragment ions were formed along the straight line between the exit of the magnet and the Mini-Ring and entered in the ring through D_1 and D_2, they could not be stored due to the mass resolution of the Mini-Ring. Therefore, compared to the initial IED in the ECR source, the stored bunch of ions had undertaken high-energy population depletion due to the dissociation processes occurring before the entrance in the ring at $t < 29$ μs. Inside the Mini-Ring, this high-energy population depletion process continued as clearly demonstrated in Fig. 3 by the fast decrease of the counts of neutral fragments during the first milliseconds of storage. For longer storage times ($t >3$ ms), the neutral counts varied much more slowly with time. We have verified by storing over 1 s (not shown here) that for $t >3$ ms the neutral count decay tended to be purely exponential with a time constant of about 300 ms, corresponding to the expected storage lifetime limitation due to collisions with the residual gas. This particular decay behavior shows that the dissociation process of the stored molecular ensemble was quenched to become negligible for $t >3$ ms and could no longer induce further high-energy population depletion (see [8]). We have estimated that under our experimental conditions the proportion of hot molecules that spontaneously dissociated inside the ring stood for less than 30% of the total stored ion population and the major part was well stored in the ring. Although other decay mechanisms, such as the electronic fluorescence or IR radiative cooling, could certainly lead to further evolution of the high-energy part of the surviving stored population distribution, their effect was indiscernible in the spectrum of neutrals when the dissociation process was nearly completely quenched.

In order to probe the time evolution of the IED, denoted by the function G(E,t) hereafter, we reheated the stored molecules by laser absorption at different storage times t_{laser}, varying from 3 to 7 ms by steps of 1 ms. The photon energy ($h\nu = 3.49$ eV) was chosen to match the electronic absorption band of the anthracene cation that has been measured in the Ar matrix at around 352 nm [40]. In response to the laser pulse, a small fraction of the stored ions absorbed one single photon leading to the formation of a reheated molecular ensemble at t_{laser}. The IED of this ensemble, denoted by $G^*(E)$, is related to $G(E, t_{laser})$ via an internal energy-dependent absorption function and a shift towards higher-energy values by hν. Although for molecules with high internal energy, up to 7 eV in the present case, the absorption cross section is unknown, it was observed to be high enough for recording spectra with good statistics. The energy dependence of the absorption cross section was not considered as a key issue in the analysis presented here, so we used a constant for its value. Also the absolute value of this cross section does not impact the analysis. It has been taken arbitrarily as unity for simplification. Therefore, $G^*(E)$ is related to $G(E, t_{laser})$ simply with an energy shift of $h\nu$, $G^*(E + h\nu) = G(E, t_{laser})$.

The fast dissociation of the reheated high-energy molecules led to a huge increase of the neutral yield at about half a revolution period (3.25 μs) after t_{laser} and a regular decrease during the first 150 μs. As an example, Fig. 4 shows a typical record of the neutral count for $t_{laser} = 3$ ms. The small and narrow peak just before the main peak is due to the noise signal on the MCP produced by the UV laser hitting the injection lens electrode. The other smaller broad and very weak peaks barely visible before t_{laser} are due to the contribution of collisions with the residual gas. In spite of the high intensity of the laser-induced peaks, their total counts were estimated to be less than 3% of the total number of stored ions. In Fig. 5 the integrated neutral yield for each revolution period is plotted as a function of time t', with $t' = t–t_{laser}$. This experimental neutral yield decay curve could not be reproduced by a simple exponential function. As discussed in several papers, e.g., [18,41], a power function ($t'^{-\alpha}$) was found to be more appropriate and the variation of the constant α under different experimental conditions provides a rough indicator of the modification of the corresponding initial IED, $G^*(E)$ [36]. Indeed, $\alpha = 1$ would be expected for an infinitely broad (flat) IED, while $\alpha < 1$ indicates that the high-energy side of the IED is in the sensitive energy window as discussed in Sec. V. For the present case ($t_{laser} = 3$ ms), the data of the first ten revolutions were fitted with a power law of exponent $\alpha = 0.87$.

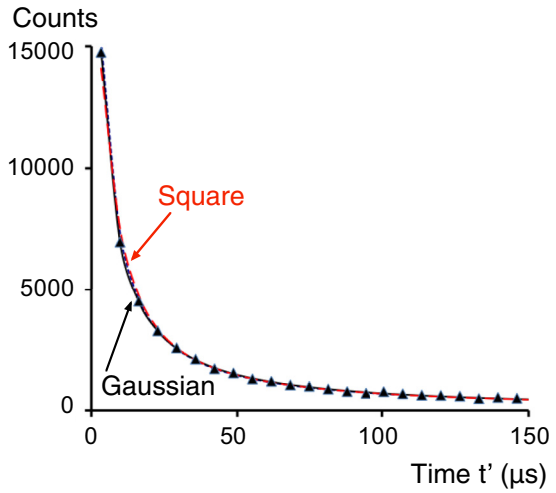

FIG. 5. (Color online) Laser-induced neutral yields as a function of $t' = t - t_{\text{laser}}$ ($t_{\text{laser}} = 3$ ms) and the adjusted decay curves using different energy population distribution profiles: long-dashed (red) line, square function; short-dashed line, power-three function; and solid line, half Gaussian shape.

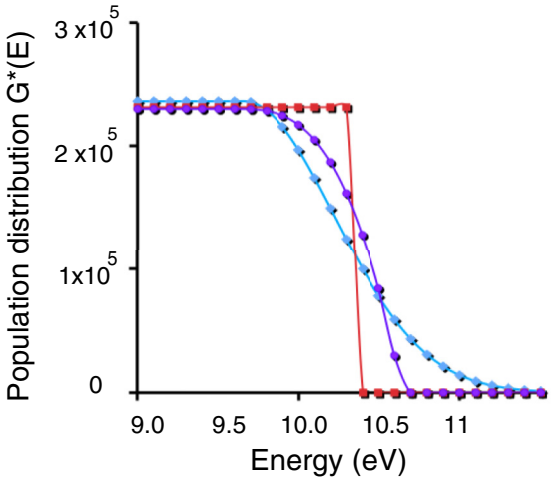

FIG. 6. (Color online) Adjusted IED $G^*(E)$ after the absorption of a single photon ($h\nu = 3.49$ eV) at $t_{\text{laser}} = 3$ ms: red squares, square function; purple circles, power-three function; and blue diamonds, half Gaussian shape.

IV. SIMULATION OF THE INTERNAL ENERGY DISTRIBUTIONS

To determine directly the time evolution of the IED $G(E,t)$ of the stored molecular ensemble, one should take into account several factors, most of them being unknown or difficult to estimate such as the initial IED in the ion source, the depletion due to dissociation, and the radiative cooling. In the following, we aim at simulating the reheated population distribution $G^*(E)$ by fitting the measured laser-induced neutral decay curves in order to model the time evolution of $G(E,t)$ before laser excitation. We postulated a mathematical shape $G^*(E)$ for the IED of the reheated molecular ensemble at $t' = 0$ with adjustable parameters. Considering that molecules of energy E might lose a neutral fragment with the dissociation rate $k_{\text{diss}}(E)$, neutral yields from molecules of the whole internal energy range were calculated as a function of t'. In the simulation, the energy scale was discretized with steps of 0.1 eV, which was sufficiently small to ensure a good and fast convergence. The values of $k_{\text{diss}}(E)$ were calculated following the work of West *et al.* [31], where the breakdown diagram of the anthracene cation was well reproduced with the fitted relation $k_{\text{diss}}(E)$. The $k_{\text{diss}}(E)$ values for typical energies are listed in Tables I. In order to fit the experimental decay curve (Fig. 5) and to evaluate the effect of the IED shape on the simulated neutral yield we have tentatively tested three

TABLE I. Dissociation lifetime τ, dissociation rate k_{diss}, and the corresponding excitation energy E of $C_{14}H_{10}^+$ according to West *et al.* [31].

τ	$k_{\text{diss}} = 1/\tau(\text{s}^{-1})$	E (eV)
25 ns	4×10^7	14
3.25 μs	3.1×10^5	10.8
29 μs	3.4×10^4	9.8
150 μs	6.7×10^3	9.2

distribution functions: a rectangular shape with a maximum energy value $E_{\max}$ defined as

$$G^*(E) = N_r \quad \text{for } E \leqslant E_{\max},$$
$$G^*(E) = 0 \quad \text{for } E > E_{\max}; \tag{1}$$

a power-3 function as used in [8] and defined as

$$G^*(E) = N_a \quad \text{for } E \leqslant E_0,$$
$$G^*(E) = N_a - Y(E - E_0)^3 \quad \text{for } E \geqslant E_0; \tag{2}$$

and a half Gaussian function defined as

$$G^*(E) = N_b \quad \text{for } E \leqslant E_1,$$
$$G^*(E) = N_b \exp[-(E - E_1)^2/2\sigma^2] \quad \text{for } E \geqslant E_1, \tag{3}$$

where $(N_r, E_{\max})$, (E_0, N_a, Y), or (E_1, N_b, σ) are parameters to be adjusted in order to fit the experimental decay curves. The fitted neutral yields and the corresponding adjusted $G^*(E)$ functions are presented in Figs. 5 and 6, respectively. At first glance, each of these shapes leads apparently to an equally good fit of the experimental decay (Fig. 5). However, a more careful analysis reveals some differences. Figure 7 displays the difference between the experimental counts and the simulated neutral yields. In the time range larger than 50 μs, the divergence was found to be comparable for the three shapes. Contrarily, for shorter times, it is much smaller for the half Gaussian shape, while larger deviations are noticed using the square and power-3 shapes. This means that the decay curve in the range from 0 to 50 μs is very sensitive to the shape of the high-energy edge of the distribution and, among the tested $G^*(E)$ functions, the half Gaussian shape with $\sigma = 0.57$ eV leads to the best fit of the experimental data.

V. SENSITIVE INTERNAL ENERGY WINDOW

From Fig. 5 it can be noticed that significant neutral yields could be detected in a time window ranging from the first half revolution period $t' = 3.25$ μs up to $t' = 150$ μs. This

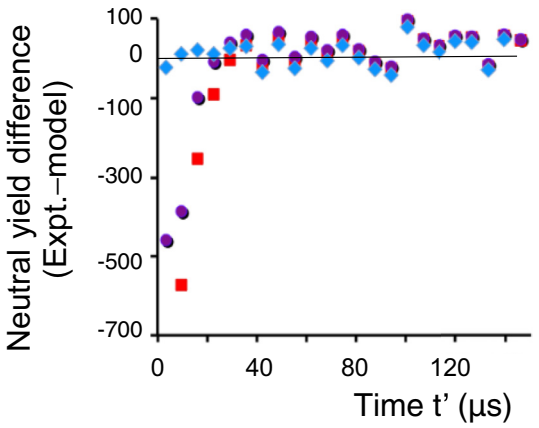

FIG. 7. (Color online) Difference between the experimental counts and the simulated neutral yields. The simulated yields were obtained using the energy distributions $G^*(E)$ of three shapes: red squares, the $G^*(E)$ square function; purple circles, the $G^*(E)$ power-three function; and blue diamonds, the $G^*(E)$ half Gaussian shape.

time window is closely related to an internal energy range for the dissociated molecules. Indeed, $t' = 3.25$ and 150 μs correspond to dissociation lifetimes of molecules with an internal energy of 10.8 and 9.2 eV, respectively (Table I). This narrow energy range is defined as the sensitive internal energy window. Any modification of the IED around 10.8 eV is expected to lead to a strong variation of the measured neutral yield, especially for the first turns. Molecules at even higher internal energy would have a very short lifetime and would have dissociated before reaching the straight line D_3-D_4, such that the emitted neutral fragments would not be detected. Therefore, any change of the IED in energy range much larger than 10.8 eV would not induce significant variation of the neutral decay curve. On the other hand, molecules with lower internal energy (<9.2 eV) would dissociate with a larger time constant (>150 μs) and the released neutrals would be dispersed over a large number of revolution periods. Hence, their contribution to the spectrum in the detection "time window" is negligible, whereas in the time range larger than 150 μs, they are drowned in the background noise due to the poor statistics. Therefore, the fitting procedure described in Sec. IV is mostly sensitive to the high-energy edge of the IEDs as long as it is located inside the sensitive internal energy window, whereas it is almost insensitive to the low energy part of the distributions. Actually, we have tested different shapes for the lower part of the energy distributions. No significant difference was observed in the simulated neutral decay curves obtained using a half Gaussian function or a full Gaussian function.

As discussed before, we assumed that the shape of the IED at $t = t_{\text{laser}}$ prior to laser excitation $G(E,t_{\text{laser}})$ is obtained from the simulated $G^*(E)$ by a simple shift of $h\nu = 3.49$ eV to lower energies, corresponding to the subtraction of the absorbed photon energy

$$\begin{aligned} G(E, t_{\text{laser}}) &= N_b \quad \text{for } E \leqslant E'_1, \\ G(E, t_{\text{laser}}) &= N_b \exp[-(E - E'_1)^2/2\sigma^2] \quad \text{for } E \geqslant E'_1, \end{aligned} \tag{4}$$

with $E'_1 = E_1 – h\nu$. In fact, by a shift of 3.49 eV to lower energy, the high-energy edge of $G^*(E)$ for $t_{\text{laser}} = 3$ ms (Fig. 6) is moved to the energy region from 6.5 to 7.5 eV. To probe the profile of the IED $G(E)$ in this region, the third harmonic of Nd:YAG provides just the right photon energy to bring the high-energy edge into the sensitive energy window. However, using the second harmonic (2.33 eV), after one-photon absorption, the high-energy edge of the IED $G^*(E)$ would be brought to an energy region that is lower than the sensitive window. So the second harmonic is not suitable for the present experiment.

Although the simulation procedure is not sensitive to the low-energy part of the distribution $G(E,t_{\text{laser}})$, experimentally, it is possible to probe the low-energy edge of the IED by bringing this low-energy region into the sensitive energy window. The following analysis illustrates roughly that idea. Neutral decay curves have been recorded at $t_{\text{laser}} = 3$ ms as a function of the laser fluence. The first ten points of each decay curve were fitted using a time-dependent power law $t^{-\alpha}$ as explained in Sec. III. Despite large error bars, the power-law exponent α displayed in Fig. 8 appears to increase slightly at full laser fluence (12 mJ/cm^2 per pulse). It is expected that two-photon-absorption events would be enhanced at increased laser fluence. This process would bring the high-energy edge of the IED to about 14 eV, way above the sensitive energy window. At such high internal energy, due to the very short dissociation lifetime (25 ns, Table I), most of the anthracene molecules would have dissociated before reaching the straight section between D_3 and D_4. Therefore, the neutral decay curve and as a consequence the exponent constant α should not be affected by the two-photon absorption process of molecules at the high-energy edge of the IED. However, the two-photon absorption process would bring populations in the low-energy region, typically around 3.5 eV, into the sensitive energy window. This may explain the observed increase of α with the laser fluence. Indeed, to probe of the low-energy edge of the IED, experiments should be designed to bring this part of the population into the sensitive energy window either by two-photon absorption or by using one photon with larger energy. This is beyond the scope of the present work.

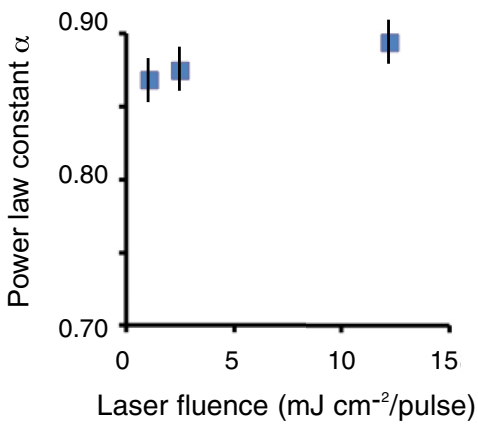

FIG. 8. (Color online) Power-law exponent α as a function of laser fluence for $t_{\text{laser}} = 3$ ms.

VI. TIME EVOLUTION OF THE INTERNAL ENERGY DISTRIBUTIONS

In order to study the time evolution of the IED as a function of the storage time, we have recorded neutral count spectra for different laser excitation times $t_{laser} = 3, 4, 5, 6$, and 7 ms under the same experimental conditions. The corresponding neutral decay curves, after corrections, are plotted in Fig. 9 as a function of t', with t_{laser} defined as the time reference $t' = 0$ in all cases. The stability of the experimental conditions might be altered by the fluctuation of the ECR ion source. It was monitored by measuring a constant total number of neutrals from 0 to 3 ms due to the spontaneous dissociation of hot molecules. In this series of experiments, the initial ion bunch time width was about 1 μs. Special care was taken to ensure the time overlap between the laser pulses and the center of the ion bunches. Nevertheless, the following experimental factors led to a progressive decrease of the number of excited molecules with increasing t_{laser}: the spread of the ion bunch during the storage time due to the initial kinetic energy dispersion of the ion beam, the initial emittance of the beam that would result in dispersion of the revolution period and a decrease in the number of stored ions with time due to collisions with the residual gas. The neutral decay curves shown in Fig. 9 were obtained from the raw decay curves recorded at different t_{laser} with corrections taking into account the above predictable factors.

Following the procedure described in Sec. IV, each decay curve was fitted using a half Gaussian shape function $G^*(E)$. It should be noticed that although the decay curves of Fig. 9 have been fitted independently, the resulting values of N_b are very similar, showing only small dispersions in a range of less than 5%. The absolute values of N_b depend on experimental parameters that have been corrected during the analysis (see the discussion above), except, however, for a possible variation of the absorption cross section. The nearly constant

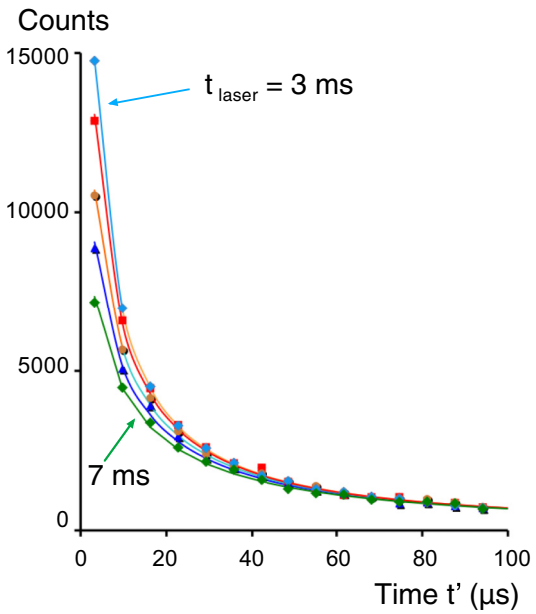

FIG. 9. (Color online) Experimental (symbols) and modeled (solid lines) decay curves versus $t' = t - t_{laser}$ after the laser pulse fired at $t_{laser} = 3, 4, 5, 6$, and 7 ms.

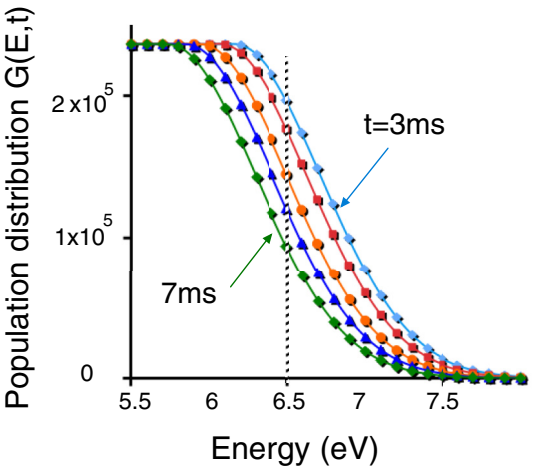

FIG. 10. (Color online) The IED of the stored ion bunches at 3, 4, 5, 6, and 7 ms of storage time.

value of N_b for different t_{laser} is tentatively interpreted as proof of the nearly constant overall absorption cross section on the time evolution of the IED. It justifies our approximation considering the absorption factor as quasi-independent of the internal energy in the studied energy region. This weak dispersion of the values of N_b will be neglected in the following. The corresponding IEDs $G(E, t = t_{laser})$ prior to laser absorption are displayed in Fig. 10.

The main feature appearing in Fig. 10 is the time evolution of the IED $G(E,t)$. The regular shift of the high-energy edge of the IED to lower energies demonstrates the existence of an efficient cooling process occurring in the observed time range from 3 to 7 ms. In the energy region around 6.5 eV, the high-energy edge was estimated to shift globally at a rate of $[\Delta E/\Delta t]_{measured} \cong -100\,\text{eV/s}$. Since the population depletion due to dissociation is negligible in this time range, the measured shift rate is attributed to radiative cooling and will be discussed in details in the following sections.

VII. FAST POPULATION DECAY RATE VERSUS INTERNAL ENERGY

From the simulated IEDs shown in Fig. 10, it is possible to extract population decay rates as a function of the excitation energy E. As an example, a vertical line was drawn at an energy value $E = 6.5$ eV in Fig. 10. It crosses all the $G(E,t_{laser})$ curves at different times corresponding to the experimental t_{laser} values. By plotting the data $G(6.5\,\text{eV},t_{laser})$ as a function of time (Fig. 11), a population decay curve of molecules whose initial internal energy was 6.5 eV is obtained. This analysis has been repeated for E varying from 6.0 to 7.4 eV by steps of 0.2 eV and the results are plotted in Fig. 11 in a semilogarithmic scale. All those decay curves could be nicely fitted by exponentials with characteristic measured population decay rates $k_{measured}$, presented in Table II. It should be kept in mind that these population decay rates were determined from the set of simulated IEDs and were not measured directly in the experiment. These rates are expected to result from the sum of contributions of all possible decay mechanisms for a molecule of internal energy E, i.e., the dissociation and the

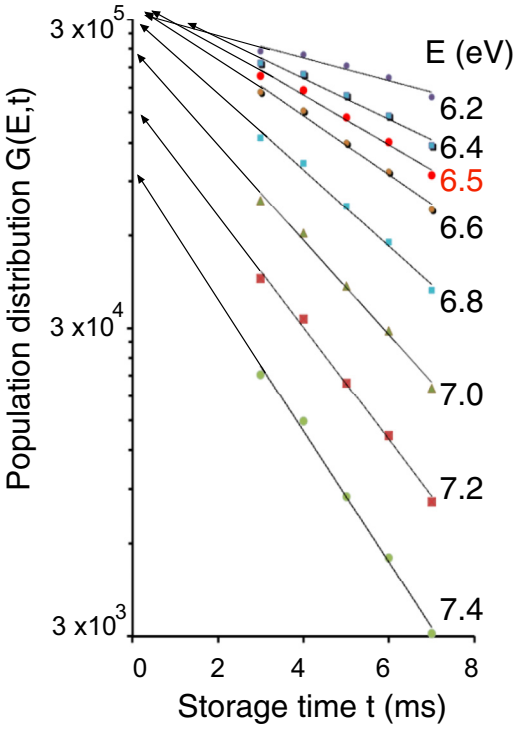

FIG. 11. (Color online) Evolution of $G(E,t)$ versus the storage time at different excitation energies from $E = 6.2$ to 7.4 eV. Each series of $G(E,t)$ values at a given value E is fitted with an exponential decay $G(E,0)\exp(-k_{\text{measured}}t)$. Arrows indicate the extrapolated value $G(E,0)$.

radiative emissions. For comparison, the dissociation rates k_{diss} from the Ref. [31] are given in Table II. In the energy range of interest $E < 7.5$ eV, k_{diss} is much smaller than k_{measured}, so the contribution of the dissociation is negligible. This is in agreement with our statement based on the analysis of the spontaneous neutral count decay (Fig. 3). The observed population decay is therefore attributed predominantly to the radiative emissions. The measured decay rates were found to be varying from 450 to 25 s^{-1} in the internal energy range from 7.4 to 6.0 eV.

TABLE II. Calculated dissociation rate k_{diss} from [31], measured population decay rate k_{measured}, and fluorescence cooling rate $\eta_{\text{cool, elec}}$ as a function of the excitation energy E before laser irradiation.

E (eV)	$k_{\text{diss}}(s^{-1})$	$k_{\text{measured}}(s^{-1})$	$\eta_{\text{cool, elec}}(s^{-1})$
8.6	1330		
8.2	368		
7.6	42		
7.4	18	450	92
7.2	9	390	83
7.0	3.4	320	71
6.8	1.2	260	60
6.6	0.4	200	48
6.4	0.1	130	32
6.2	0.04	85	22
6.0	0.01	25	7

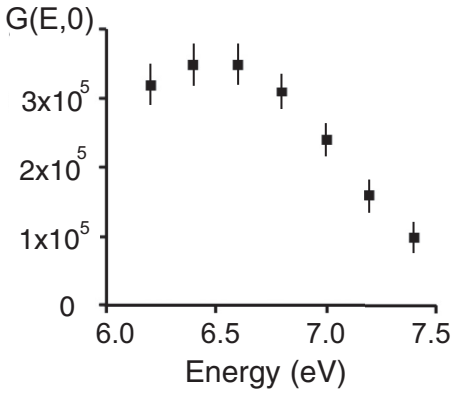

FIG. 12. Extrapolated values $G(E,t = 0)$ of the data in Fig. 11 as a function of the energy E.

From Fig. 10 one can notice that the measured population decay rate k_{measured} and the shift rate $[\Delta E/\Delta t]_{\text{measured}}$ of the high-energy edge of IED provide complementary information on the time evolution of the IED. These two measured quantities are tightly related through the IED profile $G(E,t)$. By following the time evolution of the high-energy edge of the IED along a horizontal line in Fig. 10, $G(E,t)$ stays constant, therefore $dG(E,t) = 0$. One can express the total differential $dG(E,t) = 0$ with the partial derivatives of $G(E,t)$ and obtain the relation between k_{measured} and $[\Delta E/\Delta t]_{\text{measured}}$ as

$$k_{\text{measured}} = -\frac{1}{G}\frac{\partial G}{\partial t} = \frac{1}{G}\frac{\partial G}{\partial E}\left[\frac{\Delta E}{\Delta t}\right]_{\text{measured}}. \quad (5)$$

This relation is locally linear. A fast energy shift leads to fast population decay and conversely fast population decay leads to a fast energy shift.

In Fig. 11, for each value of E, the fitted exponential function, namely, $G(E,0)\exp(-k_{\text{measured}}t)$, was extrapolated to $t = 0$. The obtained values $G(E,0)$ are displayed in Fig. 12 as a function of E. Under the hypothesis that no faster process would have modified the IED in the shorter time range $t < 3$ ms, the values $G(E,0)$ could be considered as the initial IED in the ECR source. The extrapolated values are quite constant for $6.2 \leqslant E \leqslant 6.8$ eV and exhibit a decreasing tendency with increasing energy for $E \geqslant 7$ eV. This feature is generally expected for IEDs from an ECR ion source, i.e., a rather broad distribution that depends on the ion nature and the source conditions. Although the half Gaussian function was found to be the best shape for simulating the measured neutral decay curves, this predefined shape was still a factor of approximation in the present approach. Slight dispersion of these Gaussian functions from the true IEDs would lead to large deviations of the extrapolated $G(E,0)$ values especially in the high-energy region where the corresponding decay curves were extracted from the tails of the simulated IED $G(E,t_{\text{laser}})$ (Fig. 10). To get a more precise description of the high-energy part of the IED, it would be necessary to probe the population distributions at shorter storage times or to use a more sophisticated simulation model.

VIII. RADIATIVE COOLING MECHANISMS: INFRARED AND ELECTRONIC PHOTON EMISSIONS

As mentioned in the Introduction, the radiative cooling of anthracene molecular ions can result from two different mechanisms: IR emission and/or fluorescence emission due to electronic transitions from thermally excited states. In the following sections we will discuss both mechanisms in order to determine their relative importance in the measured population decay and in the global radiative cooling of the anthracene molecular ions. These mechanisms have been described in detail for anthracene cations by Boissel *et al.* [7] and will be recalled briefly in Secs. VIII A and VIII C.

A. IR emission cooling rate

For PAH molecules (including anthracene) with excitation energy E, the IR cooling process is usually described using a statistical model. For molecules in the ground electronic state, the total internal energy E is distributed statistically among all vibrational modes ($3N$–6, N stands for the number of atoms). The emission rate $k_{i,v}$ from a specific mode i via the transition between two vibrational states $v \rightarrow v$–1 is defined as the product of the Einstein coefficient of spontaneous transition and the probability of presence in the higher state. Considering one particular molecule, the emission of an IR photon of mode i induces an energy loss via a discrete step of $h\nu_i$. In the case of anthracene, the quanta of transition energies are smaller than 0.2 eV [40]. Due to the statistical nature of the energy distribution, an average energy decreasing rate due to IR emission was therefore defined by summing over the whole set of IR transitions [7]

$$\left\lfloor \frac{dE}{dt} \right\rfloor_{\mathrm{IR}} = -\sum_i \sum_v k_{i,v} h\nu_i. \tag{6}$$

Under this model, for E much higher than the IR emission energy quanta $E \gg h\nu_i$ the internal energy of each molecule follows a rather smooth variation curve. In the same paper [7] a logarithmic IR cooling rate $\eta_{\mathrm{cool,\,IR}}$ was defined as

$$\eta_{\mathrm{cool,\,IR}} = -\frac{1}{E}\left\lfloor \frac{dE}{dt} \right\rfloor_{\mathrm{IR}}. \tag{7}$$

For anthracene, in a wide energy range from 2 to 10 eV, $\eta_{\mathrm{cool,\,IR}}$ was found to be about 2 s^{-1} and nearly energy independent (see Fig. 2 in [7]). As a consequence, in our experiment, the IR emission is expected to induce a shift of the high-energy edge of the IED of the stored anthracene ions. In the region around 6.5 eV, the high-energy edge would shift due to IR emission at a rate of $[E/\Delta t]_{IR} = -\eta_{\mathrm{cool,\,IR}} \times E \cong -13\,\mathrm{eV/s}$. This value is much smaller than the measured value of $[\Delta E/\Delta t]_{\mathrm{measured}} = -100\,\mathrm{eV/s}$ (in absolute values). To estimate the contribution of the IR emission to the variation of the IED, it is convenient to define a mean IR emission rate $\bar{k}_{\mathrm{IR}}$ by replacing the summation in Eq. (6) with a simple product $\bar{k}_{\mathrm{IR}} h\bar{\nu}_{\mathrm{IR}}$. Taking $h\bar{\nu}_{\mathrm{IR}} \approx 0.165$ eV as the mean energy of the main IR transition modes in the range from 0.15 to 0.18 eV [40], we get $\bar{k}_{\mathrm{IR}} = \frac{-[dE/dt]_{\mathrm{IR}}}{h\bar{\nu}_{\mathrm{IR}}} = \frac{\eta_{\mathrm{cool,IR}} E}{0.165} \approx 12E$ (s^{-1}), with E in eV.

Due to the energy evolution governed by the rate equation (7), the high-energy edge of an IED $G(E,t)$ varies with time through an energy variation function $G(E(t))$ for a given G value. For the fitted IED of this work, i.e., the half Gaussian shape function [Eq. (4)], the global shift of the high-energy edge to lower energies due to IR emission leads to a population decrease at a given energy E. A population decay rate $k_{\mathrm{IR}}^{\mathrm{pop}}$ can be defined in the same way as in Eq. (5),

$$k_{\mathrm{IR}}^{\mathrm{pop}} = -\frac{1}{G}\frac{\partial G}{\partial t} = \frac{1}{G}\frac{\partial G}{\partial E}\left\lfloor \frac{dE}{dt} \right\rfloor_{\mathrm{IR}} = \frac{(E - E'_1)E}{\sigma^2}\eta_{\mathrm{cool,IR}}. \tag{8}$$

It should be noted that this population decay rate should by no means be confused with the mean IR emission rate $\bar{k}_{\mathrm{IR}}$. Due to the fact that the IR emission energies are much smaller than the studied internal energy E, when considering the variation of $G(E,t)$ during Δt at a given E, one should take into account not only the decrease $\Delta G_- = \bar{k}_{\mathrm{IR}} G(E)\Delta t$ due to IR emission from molecules at the energy E but also the increase $\Delta G_+ = \bar{k}_{\mathrm{IR}} G(E + h\bar{\nu}_{\mathrm{IR}})\Delta t$ due to the IR emission from molecules at neighboring higher energies. Therefore, the IR-induced population decay rate $k_{\mathrm{IR}}^{\mathrm{pop}}$ is tightly related to the profile of the IED and particularly the partial derivative of G with respect to E, $\frac{\partial G}{\partial E}$. In an IED region where G is constant $\frac{\partial G}{\partial E} = 0$, it is expected that $\Delta G_- = \Delta G_+$, i.e., the population decrease is compensated for exactly by the population increase, therefore $k_{\mathrm{IR}}^{\mathrm{pop}} = 0$, i.e., no population decay should be observed. In a G increasing region, for example, the low-energy edge of an IED $\frac{\partial G}{\partial E} > 0$, $\Delta G_- < \Delta G_+$, i.e., the population decrease is smaller than the population increase, therefore $k_{\mathrm{IR}}^{\mathrm{pop}} < 0$ and the IR emission should lead to a population gain. Around the high-energy edge of an IED $\frac{\partial G}{\partial E} < 0$, $\Delta G_- > \Delta G_+$, i.e., the population decrease is larger than the population increase, therefore $k_{\mathrm{IR}}^{\mathrm{pop}} > 0$ and the IR emission should lead to a population decay.

B. Estimated electronic fluorescence decay rates

The measured population decay rate k_{measured} is contributed partly by the IR emission and partly by the electronic fluorescence decay. By subtracting $k_{\mathrm{IR}}^{\mathrm{pop}}$ from k_{measured}, one can get the contribution from the electronic fluorescence emissions, referred to as $k_{\mathrm{elec}}^{\mathrm{pop}}$:

$$k_{\mathrm{elec}}^{\mathrm{pop}} = k_{\mathrm{measured}} - k_{\mathrm{IR}}^{\mathrm{pop}}. \tag{9}$$

However, the determination of $k_{\mathrm{IR}}^{\mathrm{pop}}$ at a given energy value E is not straightforward. In fact, $k_{\mathrm{IR}}^{\mathrm{pop}}$ depends not only on E, but also on E'_1 [Eq. (8)], which varies in turn with time. By using Eq. (8), numerical values of $k_{\mathrm{IR}}^{\mathrm{pop}}$ were calculated for a given E at different t_{laser}. A mean value over the experimental t_{laser} range was found to be proportional to k_{measured} with a coefficient around 0.1. This coefficient coincides with the ratio between the IR induced and the measured energy shift rate $[\Delta E/\Delta t]_{\mathrm{IR}}/[\Delta E/\Delta t]_{\mathrm{measured}}$, in agreement with Eqs. (5) and (8). Therefore, the measured population decay rate due to electronic fluorescence emission was estimated by $k_{\mathrm{elec}}^{\mathrm{pop}}(E) \approx 0.9 k_{\mathrm{measured}}(E)$.

Electronic fluorescence emission is the major process leading to the population decay of molecules at a given energy value E. A fluorescence emission rate $k_{\mathrm{elec}}(E)$ is defined as a function of the internal energy. Following the model of Boissel *et al.* recalled in detail in Sec. VIII C, the fluorescence emission

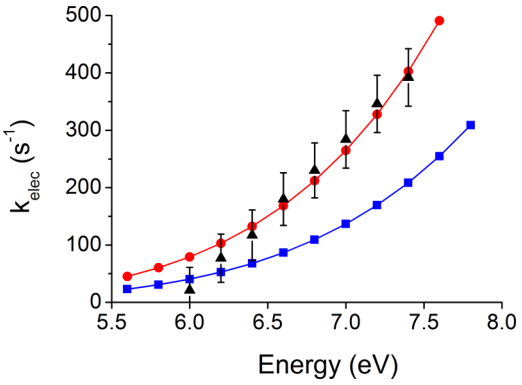

FIG. 13. (Color online) Experimental fluorescence emission rate (triangles) and the modeled rate versus the excitation energy. Theoretical values were calculated using $E_{D_2} = 1.75$ eV and $A_{\rm elec} = 7 \times 10^6$ s^{-1} (squares) or $A_{\rm elec} = 15.7 \times 10^6$ s^{-1} (circles).

process of molecules of energy E results in a sudden decrease of the internal energy in a single step from E to E–$h\nu_{\rm elec}$. This would lead to a decrease of $G(E,t)$ at energy E and its increase at lower energy E–$h\nu_{\rm elec}$. Similarly, the fluorescence emission from molecules at higher energy $E + h\nu_{\rm elec}$ should lead to an increase of $G(E,t)$ at E. The time evolution of the population at the energy E is governed by the rate equation

$$\frac{\partial G(E,t)}{\partial t} = -k_{\rm elec}^{\rm pop}\, G(E,t) = -k_{\rm elec}(E)G(E,t) + k_{\rm elec}(E + h\nu_{\rm elec})G(E + h\nu_{\rm elec},t). \quad (10)$$

To simplify the discussion, we consider the electronic transition of energy $h\nu_{\rm elec} = 1.75$ eV (see Sec. VIII C). It should be noted that for E at the high-energy edge of the IED around 6.5 eV, the value $E + h\nu_{\rm elec}$ is about 8.2 eV. In this high-energy region, the IED vanishes as shown in Fig. 10. So, the positive term in the rate equation (10) is negligible and the population decay rate $k_{\rm elec}^{\rm pop}$ coincides with $k_{\rm elec}$ at the high-energy edge of the IED,

$$k_{\rm elec}(E) \approx k_{\rm elec}^{\rm pop}(E). \quad (11)$$

The estimated electronic fluorescence emission rate $k_{\rm elec}(E)$ is plotted in Fig. 13 as a function of the internal energy E.

C. Theoretical model: Electronic fluorescence emission

Considered as a fast radiative cooling mechanism, the fluorescence emission via electronic transitions was studied by Boissel *et al.* for the anthracene cation [7]. For molecules initially in the ground electronic state, denoted by D_0, at $E_{D_0} = 0$ with high vibrational energy E, the degenerated electronic excited states, denoted by D_1, D_2,..., at E_{D_n} with vibrational energy $E - E_{D_n}$, can be populated via the inverse internal conversion. The probability of presence at such vibronic excited states can be estimated by the ratio of the density of states $\rho(E - E_{D_n})/\rho(E)$. Molecules in an electronic excited state may undergo a fast fluorescence transition with Einstein coefficients typically on the order of $10^6 - 10^7$ s^{-1}. Due to the fact that the density of state $\rho(E - E_{D_n})$ decreases dramatically with increasing E_{D_n}, the probability of an inverse internal conversion to higher electronic states ($D_n, n > 2$) can be neglected. Furthermore, the transition from the first excited electronic state (D_1) to the ground state is forbidden; the fluorescence decay occurs therefore mainly via the second electronic exited state (D_2). The corresponding rate of fluorescence emission $k_{\rm elec}$ was estimated as the sum of two terms:

$$k_{\rm elec}(E) \approx A_{\rm elec}\,\frac{\rho(E - E_{D_2})}{\rho(E)} + A_{\rm elec,\,1}\,\frac{\rho(E - E_{D_2} - h\nu_1)}{\rho(E)}. \quad (12)$$

The first term is the product of the Einstein coefficient $A_{\rm elec}$ by the probability of presence in the electronic excited state D_2 with vibrational energy $E - E_{D_2}$. This term corresponds to the dominant pure electronic transition of energy $h\nu_{\rm elec} = E_{D_2}$ without implying variation of quantum numbers of any vibrational oscillators, namely, $\Delta v_i = 0$. In Ref. [7] the second term takes into account the vibronic transition of energy $h\nu_{\rm elec} = E_{D_2} + h\nu_1$ with the decrease of one unit of the quantum number of a particular mode $\Delta v_1 = -1$, denoted arbitrarily by the mode number 1. Its contribution to $k_{\rm elec}$ corresponds to about 10% of the first term. Contributions from similar transitions implying other modes with larger vibrational energies $h\nu_i$ correspond to less than 1% of the total $k_{\rm elec}$ [7]. These extra terms are neglected in Eq. (12). To calculate the theoretical value of the fluorescence emission rate $k_{\rm elec}$, accurate values of E_{D_2} and $A_{\rm elec}$ are needed. First, for the electronic state D_2, several values can be found in the literature. Using the Gaussian software with the B3LYP functional, Sanchez-Carrera [42] calculated a value of 1.68 eV. A value of 1.7 eV was used by Boissel *et al.* [7]. In an experimental work, a larger value of 1.75 eV was obtained in the gas phase by Sukhorukov *et al.* [43]. This last value will be used in the following because it was measured under conditions more comparable to the present work, i.e., in the gas phase without a matrix shift as in previous studies [40]. The values of $k_{\rm elec}$ calculated with Eq. (12), $E_{D_2} = 1.75$ eV, and $A_{\rm elec} = 7 \times 10^6$ s^{-1}, as well as $h\nu_1 \approx 1331$ cm^{-1} and $A_{\rm elec,\,1} = 3.2 \times 10^6$s^{-1} as in Ref. [7], are shown in Fig. 13. These values are much smaller than our estimated electronic fluorescence emission rates. To reproduce the measured $k_{\rm elec}(E)$ values with the theoretical model, a larger value of $A_{\rm elec}$ is needed. Indeed, using $A_{\rm elec} = 15.7 \times 10^6$ s^{-1}, the theoretical values calculated using Eq. (12) gives the best fit of the experimental data as shown in Fig. 13. This $A_{\rm elec}$ value is about twice that used in the work of Boissel *et al.* [7].

The enhancement of the fitted $A_{\rm elec}$ can be interpreted as follows. It is noteworthy that in Ref. [7] the Einstein coefficients $A_{\rm elec}$ of the spontaneous emission channels of D_2 were obtained from the optical absorption spectra of the anthracene cation trapped in an Ar matrix at 12 K [40]. In such experiments, only allowed transitions from the ground electronic and vibrational states ($D_0, v_i = 0$ for all modes i) to vibronic levels (D_2, v_i') were measured. The absorption lines include the main line with $\Delta v_i = 0$ leading to $v_i' = 0$ and the high-energy band composed of weaker lines with $\Delta v_i > 0$ leading to $v_i' = 1$ or 2 for several specific modes. The low-energy band implying transitions with $\Delta v_i < 0$ is forbidden in such an absorption spectrum. For the electronic spontaneous emission from D_2 to D_0, the reverse transitions of the absorption lines were considered in Ref. [7]. Indeed, the

first term in Eq. (12) corresponds to the main absorption line with $\Delta v_i = 0$; the second term in Eq. (12) and other negligible terms in Ref. [7] correspond to the contribution of lines appearing in the high-energy band of the absorption spectrum. However, these terms represent only a part of the allowed spontaneous emission routes. In fact, emissions leading to lines in the low-energy band, which are absent in the absorption spectrum, may be allowed in the spontaneous transitions, notably, transitions from initial vibronic states (D_2, v_i') to (D_0, v_i) with $v_i = v_i' + 1$ or $v_i' + 2$ for several modes while $v_i = v_i'$ for most of the modes. To estimate the contribution of the low-energy band in the spontaneous emission spectrum, we have performed a theoretical calculation using the linear-response time-dependent density-functional theory [44,45] approach with the CAM-B3LYP [46] functional and the 6311++G (2df,2pd) basis set. As a first approximation, we have estimated the spontaneous transition rate from $(D_2, v_i' = 0)$ to $(D_0, v_i = 0)$ simulating the main emission channel with $\Delta v_i = 0$ and the total A_{elec} including contributions from all possible spontaneous transition channels with $v_i >= v_i'$. The total A_{elec} was found to be about twice that of the route only taking into account $\Delta v_i = 0$. This explains the disagreement between our fitted value A_{elec} and the value used in Ref. [7]. Indeed, in that work, the electronic fluorescence emission rate k_{elec} was underestimated due to the omission of the low-energy band in the spontaneous emission channels with $v_i > v_i'$.

D. Fluorescence cooling rate

To estimate the contribution of the fluorescence emission to the cooling of a molecular ensemble of a given initial internal energy E, one should consider both the fluorescence emission rate and the energy carried by the emitted photons. Although for each molecule the internal energy varies in large discrete steps via electronic transitions, it is informative and meaningful to proceed in an analogous way as for the IR emission by calculating the variation rate $[\frac{dE}{dt}]_{\text{elec}}$ of the average energy per molecule to determine a mean fluorescence cooling rate $\eta_{\text{cool, elec}}$ [7],

$$\eta_{\text{cool, elec}} = -\frac{1}{E}\left[\frac{dE}{dt}\right]_{\text{elec}} \approx \frac{E_{D_2}}{E}\, k_{\text{elec}}. \qquad (13)$$

Similarly to IR emission, the average energy variation rate $[\frac{dE}{dt}]_{\text{elec}}$ approximated by $-E_{D_2} k_{\text{elec}}$ corresponds to the ratio of the total power emitted via electronic transitions and the number of molecules in the ensemble. It is noteworthy that $[\frac{dE}{dt}]_{\text{elec}}$ is different from the shift rate of the high-energy edge of the IED induced by the fluorescence emission. Indeed, similar to Eq. (5), the high-energy edge shift rate is proportional to $[\frac{dE}{dt}]_{\text{elec}}$ through a coefficient that depends on the partial derivative of $G(E,t)$ with respect to E. For the fitted half Gaussian shape functions [Eq. (4)], the coefficient is given by $\sigma^2/(E - E_1')E_{D_2}$. The mean fluorescence cooling rate $\eta_{\text{cool, elec}}$, presented in Table II, was calculated with Eq. (13) using k_{elec} values estimated from the measured population decay rate after corrections of the IR emission effect. Here $\eta_{\text{cool, elec}}$ ranges from 7 to 92 s^{-1} for internal energies in the range from 6 to 7.4 eV. These values are much larger than the theoretical IR cooling rate $\eta_{\text{cool, IR}}(2\,\text{s}^{-1})$ calculated in this energy region [7]. So, for anthracene ions, in our investigated energy range, the fluorescence emission via electronic transition is found to be a more efficient radiative cooling channel. This is due not only to the increase of the fluorescence emission rate k_{elec} with the excitation energy but also to the larger energy carried by a single photon.

IX. CONCLUSION

In summary, using an ECR ion source and a small electrostatic storage device Mini-Ring, we have measured the radiative-emission-induced population decay rate of anthracene cations with internal energy from 6 to 7.4 eV by following the time evolution of the simulated IEDs in the time range from 3 to 7 ms. In the investigated internal energy range, the fluorescence emission rate k_{elec} has been estimated and found to strongly increase from 23 to 400 s^{-1}. These values are larger than the prediction based on the theoretical model of Boissel *et al.* [7]. Nevertheless, the experimental fluorescence emission rates k_{elec} were well simulated using the model of Boissel *et al.* with a modified value of A_{elec} that had to be increased by a factor of 2. This enhancement of the Einstein coefficient A_{elec} of the excited states is interpreted by the addition of contributions from the low-energy band in the expected spontaneous emission spectrum. This band, due to transitions from (D_2, v_i') to (D_0, v_i) with $v_i > v_i'$, is absent in the absorption spectrum. The total Einstein coefficient of the state $(D_2, v_i' = 0)$ was calculated theoretically. It was found that by including the low-energy band, the value of A_{elec} was indeed increased by about a factor of 2 compared to that of the main origin line with $\Delta v_i = 0$. This is in good agreement with our interpretation.

The fluorescence cooling rates $\eta_{\text{cool, elec}}$ were also estimated and compared with the theoretical IR cooling rate. We found that for $E > 6$ eV the fluorescence emission is the dominant radiative cooling channel. In spite of the statistically very low probability of presence in the electronic excited states, the relatively high fluorescence cooling rate is explained by the high spontaneous transition rate of the involved states and the large quantity of energy carried by a single photon. A similar mechanism has been observed in the cooling of larger systems such as C_{60} and explained as due to the transition of thermally excited electrons, involving the energy transfer from vibrational to electronic excitation. This process is very sensitive to the energy gap between the first electronic excited states and the ground state and therefore it is expected to depend strongly on the charge and size of PAHs. Confirmation of this effect has been provided by the study of the cooling of C_6^- and C_6H^- [17]. The very different radiative cooling rates measured for these two cations were explained by their different electronic structure, especially by the different energy for their first excited states.

The application of the present experimental method to other molecules of the PAH family with different charge states is left for future work. The enhancement or absence of this fast electronic cooling mechanism may have important consequences for the presence of particular PAHs in the ISM. Experiments using other small- and medium-sized PAH molecules such as naphthalene, pyrene, and coronene have been performed [47]. This work also demonstrates the potential of the new generation of small ESR for measuring

the radiative decay rate of molecular ions. Other diagnostics being developed for the Mini-Ring include the detection of neutrals after a shorter delay time following laser excitation to gain more information on the high energy edge of the IED and the coincidence measurement of charged and neutral fragments versus the storage time to identify the fragmentation channels (time-resolved daughter mass spectrometry). This ring provides therefore an excellent tool for probing the relaxation dynamics of large molecular systems such as PAHs.

ACKNOWLEDGMENTS

We thank F. Lepine, I. Compagnon, and C. Bordas (Institut Lumière Matière) for useful discussions about the statistical model, thermal emission, and the photoelectron detachment process. We also thank this group for support with the pulsed UV 1-kHz laser (Spectra-Physics) (supported by Agence Nationale de la Recherche (ANR) through Project No. ANR-06-BLAN-0041). This work was supported by the ANR Program No. ANR-10-BLAN-0426 "Anneau."

[1] A. Leger and J. Puget, Astron. Astrophys. **137**, L5 (1984).
[2] L. Allamandola, A. Tielens, and J. Barker, Astrophys. J. **290**, L25 (1985).
[3] *PAHs and the Universe*, edited by C. Joblin and A. G. G. M. Tielens, EAS Publications Series Vol. 46 (EDP Sciences, France, 2011).
[4] A. G. G. M. Tielens, Rev. Mod. Phys. **85**, 1021 (2013).
[5] A. Léger, P. Boissel, and L. d'Hendecourt, Phys. Rev. Lett. **60**, 921 (1988).
[6] A. Léger, P. Boissel, F. Desert, and L. d'Hendecourt, Astron. Astrophys. **213**, 351 (1989).
[7] P. Boissel, P. de Parseval, P. Marty, and G. Lefevre, J. Chem. Phys. **106**, 4973 (1997).
[8] S. Martin, J. Bernard, R. Brédy, B. Concina, C. Joblin, M. Ji, C. Ortega, and L. Chen, Phys. Rev. Lett. **110**, 063003 (2013).
[9] Q. Meng and H.-D. Meyer, J. Chem. Phys. **138**, 014313 (2013).
[10] J. U. Andersen, C. Gottrup, K. Hansen, P. Hvelplund, and M. O. Larsson, Eur. Phys. J. D **17**, 189 (2001).
[11] K. Hansen and E. E. B. Campbell, J. Chem. Phys. **104**, 5012 (1996).
[12] A. E. K. Sundén, M. Goto, J. Matsumoto, H. Shiromaru, H. Tanuma, T. Azuma, J. U. Andersen, S. E. Canton, and K. Hansen, Phys. Rev. Lett. **103**, 143001 (2009).
[13] M. Lange, M. W. Froese, S. Menk, D. Bing, F. Fellenberger, M. Grieser, F. Laux, D. A. Orlov, R. Repnow, T. Sieber, Y. Toker, R. von Hahn, A. Wolf, and K. Blaum, New J. Phys. **14**, 065007 (2012).
[14] Y. Toker, O. Aviv, M. Eritt, M. L. Rappaport, O. Heber, D. Schwalm, and D. Zajfman, Phys. Rev. A **76**, 053201 (2007).
[15] M. Goto, A. E. K. Sundén, H. Shiromaru, J. Matsumoto, H. Tanuma, T. Azuma, and K. Hansen, J. Chem. Phys. **139**, 054306 (2013).
[16] K. Najafian, M. S. Pettersson, B. Dynefors, H. Shiromaru, J. Matsumoto, H. Tanuma, T. Furukawa, T. Azuma, and K. Hansen, J. Chem. Phys. **140**, 104311 (2014).
[17] G. Ito, T. Furukawa, H. Tanuma, J. Matsumoto, H. Shiromaru, T. Majima, M. Goto, T. Azuma, and K. Hansen, Phys. Rev. Lett. **112**, 183001 (2014).
[18] K. Hansen, J. U. Andersen, P. Hvelplund, S. P. Møller, U. V. Pedersen, and V. V. Petrunin, Phys. Rev. Lett. **87**, 123401 (2001).
[19] H. T. Schmidt, H. Cederquist, J. Jensen, and A. Fardi, Nucl. Instrum. Methods Phys. Res. Sect. B **173**, 523 (2001).
[20] O. Aviv, Y. Toker, M. Errit, K. G. Bhushan, H. B. Pedersen, M. L. Rappaport, O. Heber, D. Schwalm, and D. Zajfman, Rev. Sci. Instrum. **79**, 083110 (2008).
[21] J. Bernard, B. Wei, A. Bourgey, R. Brédy, L. Chen, M. Kerleroux, S. Martin, G. Montagne, A. Salmoun, and B. Terpend-Ordacière, Nucl. Instrum. Methods Phys. Res. Sect. B **262**, 105 (2007).
[22] C. R. Calvert, L. Belshaw, M. J. Duffy, O. Kelly, R. B. King, A. G. Smyth, T. J. Kelly, J. T. Costello, D. J. Timson, W. A. Bryan, T. Kierspel, P. Rice, I. C. E. Turcu, C. M. Cacho, E. Springate, I. D. Williams, and J. B. Greenwood, Phys. Chem. Chem. Phys. **14**, 6289 (2012).
[23] P. Reinhed, A. Orbán, S. Rosén, R. D. Thomas, I. Kashperka, H. A. B. Johansson, D. Misra, A. Fardi, L. Brännholm, M. Björkhage, H. Cederquist, and H. T. Schmidt, Nucl. Instrum. Methods Phys. Res. Sect. A **621**, 83 (2010).
[24] V. Lepère, I. M. Ismail, M. Barat, J. A. Fayeton, Y. J. Picard, K. Wohrer, C. Jouvet, and S. Martrenchard, J. Chem. Phys. **123**, 174307 (2005).
[25] L. H. Andersen, O. Heber, and D. Zajfman, J. Phys. B **37**, R57 (2004).
[26] L. H. Andersen, T. Andersen, and P. Hvelplund, Adv. At. Mol. Opt. Phys. **38**, 155 (1997).
[27] J. Bernard, G. Montagne, R. Brédy, B. Terpend-Ordacière, A. Bourgey, M. Kerleroux, L. Chen, H. T. Schmidt, H. Cederquist, and S. Martin, Rev. Sci. Instrum. **79**, 075109 (2008).
[28] R. D. Thomas *et al.*, Rev. Sci. Instrum. **82**, 065112 (2011).
[29] Y. Ling and C. Lifshitz, J. Phys. Chem. A **102**, 708 (1998).
[30] R. Brédy, C. Ortéga, M. Ji, J. Bernard, L. Chen, G. Montagne, and S. Martin, Phys. Scr. **T156**, 014042 (2013).
[31] B. West, A. Sit, S. Mohamed, C. Joblin, V. Blanchet, A. Bodi, and P. M. Mayer, J. Phys. Chem. A **118**, 9870 (2014).
[32] N. Takahashi, Y. Adachi, M. Saito, and Y. Haruyama, Nucl. Instrum. Methods Phys. Res. Sect. B **315**, 51 (2013).
[33] B. L. Peko and T. M. Stephen, Nucl. Instrum. Methods Phys. Res. Sect. B **171**, 597 (2000).
[34] Y. Ling, Y. Gotkis, and C. Lifshitz, Eur. Mass Spectrom. **1**, 41 (1995).
[35] J. Laskin and C. Lifshitz, J. Mass Spectrom. **36**, 459 (2001).
[36] M. Ji, R. Brédy, L. Chen, J. Bernard, B. Concina, G. Montagne, A. Cassimi, and S. Martin, Phys. Scr. **T156**, 014091 (2013).
[37] Y. Ho, Y. Yang, S. Klippenstein, and R. Dunbar, J. Phys. Chem. **99**, 12115 (1995).
[38] B. West, C. Joblin, V. Blanchet, A. Bodi, B. Sztáray, and P. M. Mayer, J. Phys. Chem. A **116**, 10999 (2012).
[39] P. M. Mayer, V. Blanchet, and C. Joblin, J. Chem. Phys. **134**, 244312 (2011).
[40] J. Szczepanski, M. Vala, D. Talbi, O. Parisel, and Y. Ellinger, J. Chem. Phys. **98**, 4494 (1993).
[41] J. U. Andersen, H. Cederquist, J. S. Forster, B. A. Huber, P. Hvelplund, J. Jensen, B. Liu, B. Manil, L. Maunoury,

S. B. Nielsen, U. V. Pedersen, H. T. Schmidt, S. Tomita, and H. Zettergren, Eur. Phys. J. D **25**, 139 (2003).

[42] R. S. Sánchez-Carrera, V. Coropceanu, D. A. da Silva Filho, R. Friedlein, W. Osikowicz, R. Murdey, C. Suess, W. R. Salaneck, and J.-L. Brédas, J. Phys. Chem. B **110**, 18904 (2006).

[43] O. Sukhorukov, A. Staicu, E. Diegel, G. Rouillé, T. Henning, and F. Huisken, Chem. Phys. Lett. **386**, 259 (2004).

[44] E. Runge and E. K. U. Gross, Phys. Rev. Lett. **52**, 997 (1984).

[45] M. E. Casida, in *Recent Advances in Density Functional Methods Part I*, edited by D. P. Chong (World Scientific, Singapore, 1995), p. 155.

[46] T. Yanai, D. P. Tew, and N. C. Handy, Chem. Phys. Lett. **393**, 51 (2004).

[47] C. Ortéga, R. Brédy, L. Chen, J. Bernard, M. Ji, G. Montagne, A. R. Allouche, A. Cassimi, C. Joblin, and S. Martin, J. Phys. Conf. Ser. **583**, 012038 (2015).